Colorado School of Mines

Electrochemical Systems Engineering - 570

Class Project Report

Liam Witteman

Parametric study on bipolar membrane hydration in a CO_2 electrolyzer

Written for Dr. Steven DeCaluwe

12/15/2020

1. Introduction

Industrial processes and fossil power-plant sources emit an estimated 35 billion tons CO_2/yr [1]. To effectively curb the CO_2 emission or recycle CO_2 for economic purposes, CO_2 can be converted into hydrocarbon fuel or materials. Various power sources need energy feedstocks from liquid fuels such as gasoline, diesel, and jet fuel, which can be used in transportation on ground, in water, or for aviation. Direct CO_2 reduction (CO2R) through electrolysis is a promising technology to synthesize the hydrocarbon fuel or materials using renewable electricity [2]. The electrochemical process can be tailored based on the catalyst used and applied electric potentials, leading to a variety of different carbon products as shown by the work of Hori [3]. Ultimately, the CO_2 electrochemical reactor can be co-located with CO_2-generating sources; then, using locally produced renewable electricity, a judiciously selected catalyst, and specific operating conditions, it can produce a fuel (methanol, diesel) or chemical (ethylene, 2,3-furandiol) suited for the regional economy [4].

Rudimentary CO2Es have been demonstrated at the laboratory scale, but current densities need to go beyond mA/cm^2 to A/cm^2 to be relevant. The technology will have to draw analogies from the polymer-electrolyte membrane (PEM) water electrolysis industry to demonstrate such power. The PEM systems are modular by design and can be mass-produced commercially at the MW level. CO2Es will need to achieve the same scale to consider being coupled with the scale of CO_2 point sources such as ethanol biorefineries.

One challenge of a CO2E is the mass-transport capability of getting a gaseous reactant to a solid/liquid interface at a high rate for adequate electrochemical reaction rate. Most studies on CO2R catalyst performance have been performed in an H-cell with a pH-buffered liquid electrolyte, which is a cell condition that lacks scalability. Liquid-based cathode systems are up against the solubility limits of CO_2, which at ~30 mM can only support current densities up to 60 mA/cm^2 with vigorous stirring [5]. Such configurations are limited by mass (CO_2) transport, offering limited information on catalyst kinetics. More groups are recognizing this critical issue in aqueous-based CO2R and have begun incorporating a gas-diffusion electrode (GDE) as the cathode (allowing gas-phase CO_2 to be fed) and demonstrated current densities have risen to 100s of mA/cm^2 [6–10]. However, most of these devices are still not scalable membrane electrode assemblies (MEAs) because they contain a flowing carbonate-based liquid electrolyte in the cathode compartment as well as carbonate or hydroxide in the anode compartment.

Another challenge is the membrane choice for the environment within a CO2E. Most demonstrations use Nafion to keep the reduced products from diffusing to the anode, where their oxidation is kinetically and thermodynamically favored over water oxidation. The use of Nafion also hinders the oxygen evolution reaction (OER) on the anode because the OER proceeds most efficiently under alkaline conditions. As a result, the use of an alkaline anolyte such as KOH has been deployed to employ non-noble metal catalysts. However, under such operation, K+ ions disproportionately carry the charge because of their comparatively high concentration (1 M) and lead to an increase in potential (at constant current density) due to pH drift [11].

The shortcomings of using a CEM or AEM alone has sparked interest in employing BPM cells [8, 12–15]. The key advantage of using a BPM is the ability to maintain a pH gradient through the dissociation of water at the BPM interface as illustrated in Figure 1. CO2E cell performance relies on water balance and transport to the interfacial layer sandwiched between the AEM and CEM for adequate performance of a CO_2 electrolyzer.

Studying water transport toward the interface between the BPM provides insights on one of the potential limiting factors to increase the current density of CO2R to practical usage. Therefore, this work provides a rudimentary 1-D model that simulates charge transport, species transport, and water transport through the BPM. Important parameters for maintaining hydration in the BPM are highlighted and discussion is provided around focal points for future experimental work.

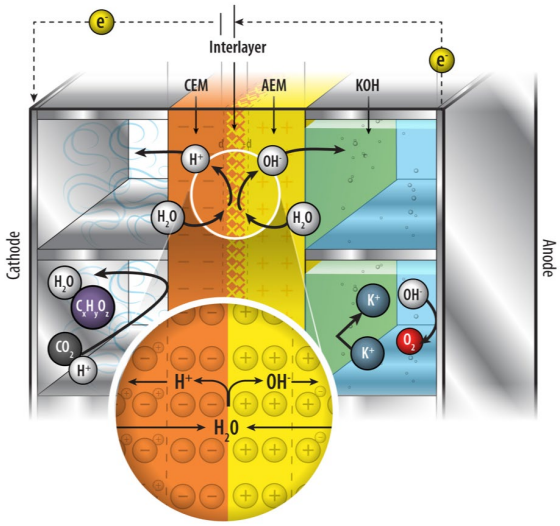

Figure 1. Working principle of a bipolar membrane in a CO2E.

2. Model Formulation

The model uses a finite-volume approach to solve conservation equations in the gas diffusion layers, catalyst layers, and bipolar membrane. A 1-D porous flux expression is utilized to solve the species transport within the gas diffusion layers and catalyst layers. Water fluxes from the catalyst layers to the BPM junction are used to solve the water hydration number (λ), accounting for diffusion and electro-osmotic drag.

The model domain is from the cathode flow channel-GDL interface to the anode GDL-flow channel interface. The time-based derived conservation equations are solved numerically on a model domain discretized at each layer's interface. The transient equations for the processes are evaluated at constant current densities and integrated over a long time span until steady state is achieved (100 s). The model captures the following physical phenomena: (i) Gas phase convection and diffusion transport in porous media, (ii) Electrochemical processes in the catalyst layer and bipolar membrane junction, (iii) electrical ohmic resistance in the GDL and CL and ionic ohmic resistance in the CEM and BPM as a function of water hydration, and (iv) water transport through the CEM and AEM. While the anode is illustrated in the modeling domain, the species transport was not explicitly modeled. This is because the cathode side employs a humidified CO_2 feed stream so it was assumed that any membrane drying would occur first at the cathode side (PEM side).

2.1 Model Assumptions

The following assumptions were utilized in the model:

1) Isothermal operation.
2) Only gas phase water on the cathode side
3) Constant water hydration number at the anode CL-AEM interface with a liquid equilibrated AEM.
4) Constant species concentration at the cathode flow channel-GDL interface.
5) Gas phase species treated as an ideal gas.
6) Silver catalyst in the cathode leading to only CO production.
7) Uniform geometric and microstructural properties in the GDL and CL.
8) Uniform potential through the CL.

2.2 Charge Transport

The conservation of charge is derived from the electrolyte-double layers in a similar fashion to [12]:

$$i_{dl} = \pm i_{ext}\frac{A_{geo}}{A_{surf}} - i_{Far} \tag{1}$$

Where we name the geometric factor A_{fac}:

$$A_{fac} = \frac{A_{geo}}{A_{surf}} = \frac{3(1-\varepsilon_{Cl}^{\circ})}{r_{CL,p}} \tag{2}$$

The sign on the current depend on whether we deal with the current of anode. Here, positive current is considered moving positive charge to the anode and negative charge to the cathode. The double layer current (i_{dl}) and Faradaic current (i_{Far}) both move positive charge from the electrode to the electrolyte bull interior.

Defining the charge separation as $q_{dl} = q_{el} - q_{elyte}$ and $\Delta\phi_{dl} = \phi_{el} - \phi_{elyte}$:

$$\frac{d\Delta\phi_{dl}}{dt} = \frac{d(\phi_{el}-\phi_{elyte})}{dt} = \frac{i_{dl}}{C_{dl}} = \frac{1}{C_{dl}}\left(\pm i_{ext}A_{fac} - i_{Far}\right) \tag{3}$$

A close view of the catalyst of the anode and cathode with the current convention is shown in Figure 2.

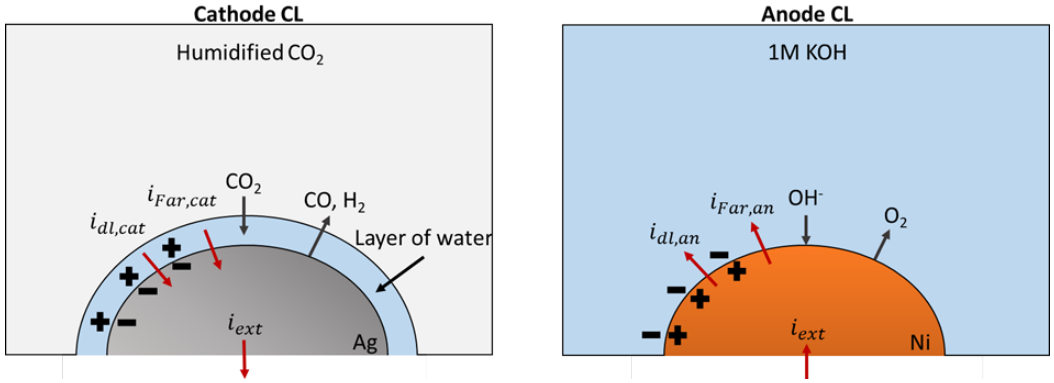

Figure 2. Close view of current convention in the catalyst layers.

The Faradaic current is calculated from Butler-Volmer's equation:

$$i_{Far} = i_{o,an/ca}\left[\exp\left(\frac{\beta_{fwd}F\eta}{RT}\right) - \exp\left(-\frac{\beta_{rev}F\eta}{RT}\right)\right] \tag{4}$$

Where the exchange current density (i_o) is modeled using an Arrhenius expression:

$$i_{o,an/ca} = A_{an/ca}\exp\left(-\frac{E_{A,an/ca}}{RT}\right) \tag{5}$$

2.3 Nernst Potential

The potential of a CO_2 electrolyzer cell is the sum of the electrode potentials and the bipolar-membrane junction potential.

$$\phi_{OCV} = \phi_{ca} - \phi_{an} - \Delta\phi_j \tag{6}$$

In the anode the oxygen evolution reaction in alkaline environment with the relevant reversible potential expression [13]:

$$2OH^- \rightarrow \frac{1}{2}O_2 + H_2O + 2e^- \qquad \phi^\circ_{an} = -0.401\,V\ vs.SHE \tag{7}$$

In the cathode the CO2R with the reversible potential expression [17]:

$$CO_2 + 2H^+ + 2e^- \rightarrow CO + H_2O \qquad \phi^\circ_{ca} = -0.11\,V\ vs.SHE \tag{8}$$

To adjust the standard-state reversible potentials, the activities are considered:

$$\phi_{an/ca} = \phi^\circ_{an/ca} - \frac{RT}{nF}\ln\left(\prod_k a_k^{v_j}\right) \tag{9}$$

Where a_k is the activity of species k and v_i is the stoichiometric coefficient of reaction j.

The water-disassociation at the CEM|AEM interface adds a junction potential that can be described as [13]:

$$2H_2O \rightarrow 2H^+ + 2OH^- \qquad \Delta\phi_j = -0.828\,V\ vs.SHE \tag{10}$$

2.4 Water Transport in BPM

The water flux from the catalyst layer to the BPM junction is governed by diffusion and electro-osmotic drag. The modes of transport for CEM and AEM are analogous so the following discussion will be for PEM and will apply for AEM. The flux of water (J_w) is based on the gradient in mass fraction of water in the membrane (f_w) and electro-osmotic drag [18-20]:

$$J_w = -\frac{\rho_{dry}}{M_w}\frac{D_{w,mem}}{1+f_w}\nabla f_w + n_{d,w}\frac{i_{io}}{F} \tag{11}$$

Where ρ_{dry} is the dry membrane density, M_w is the molecular weight of water, $D_{w,mem}$ is the water diffusion coefficient in the membrane, and $n_{d,w}$ is the electro-osmotic drag coefficient.

The mass fraction of water in the membrane is defined as:

$$\lambda = \frac{f_w}{M_w \cdot IEC} \tag{12}$$

Where IEC is the ion-exchange capacity of the membrane.

To convert J_w to a time derivative for the model the definition of λ is utilized:

$$\lambda = \frac{mol\ H_2O}{mol\ SO_4^-} \tag{13}$$

The moles of side chain groups ($e.g.\ SO_4^-$ for PEM) can be expressed as:

$$n_{SO_4^-} = c_{SO_4^-}A_{cell}\delta_j \tag{14}$$

Where $c_{SO_4^-}$ is the concentration of the side chain groups in the membrane and δ_j is the thickness of the BPM junction area.

Combining equations 11,13, and 14 results in the following time derivative:

$$\frac{\partial\lambda}{dt} = \frac{\left(-\frac{\rho_{dry}}{M_w}\frac{D_{w,mem}}{1+f_w}\nabla f_w + n_{d,w}\frac{i_{io}}{F}\right)}{c_{SO_4^-}\delta_j} \tag{15}$$

The membrane properties $D_{w,mem}$ and $n_{d,w}$ are a function of λ and taken from the work of Springer et al. for PEM [21]. The water content for PEM is based on the water activity, which is defined for PEM as:

$$a_{w,PEM} = \frac{P_{H_2O}}{P_{w,sat}} \tag{16}$$

For AEM, the literature is still in its infancy, so correlations are not well established for liquid equilibrated AEM and vary across research groups [22-24]. Therefore, the following was assumed:

$$a_{w,AEM} = \frac{\lambda}{\lambda_{sat}} \tag{17}$$

Where λ_{sat} is the water content of AEM fully equilibrated with liquid water.

The $D_{w,mem}$ and $n_{d,w}$ for AEM are used as variable parameters. The BPM junction will also act as a water sink and is assumed to have no kinetic limitations, i.e.:

$$R_{H_2O,j} = -\frac{i_{io}}{F} \tag{18}$$

2.5 Gas-Phase Transport

The conservation of species is expressed as:

$$\frac{\partial c_k}{\partial t} = -\nabla J_k + A_{frac}\dot{s}_k \tag{19}$$

Where J_k is the species mole flux, and $\dot{s}_k$ is the molar production rate.

The molar production rate is related to a charge transfer reaction j:

$$\dot{s}_{k,j} = \frac{v_{k,j} i_{Far}}{nF} \tag{20}$$

The molar flux due to convection and diffusion is expressed as:

$$J_k = C_k\left(-\frac{K_g}{\mu}\nabla P - D_{k_1k_2}^{eff}\nabla X_k\right) \tag{21}$$

Where K_g is the gas phase permeability calculated from the Kozenzy-Carman relationship, P is the pressure, D_{k_1,k_2}^{eff} is the effective binary diffusion coefficient between species k_1 and k_2, and X_k is the mole fraction of species k.

The estimation of the binary diffusion coefficient can be done by the following expression [25]:

$$\frac{pD_{AB}}{(p_{cA}p_{cB})^{1/3}(T_{cA}T_{cB})^{5/12}\left(\frac{1}{M_A}+\frac{1}{M_B}\right)^{1/2}} = a\left(\frac{T}{\sqrt{T_{cA}T_{cB}}}\right)^b \tag{22}$$

Where p is pressure in atm, T is temperature in Kelvin, p_c is the critical pressure of species A or B, T_c is the critical temperature of species A or B, and M is the molecular weight of species A or B. The coefficients a and b are experimentally derived from being $a = 1.3640\times10^{-4}$ and $b = 2.334$ for a binary mixture with water.

The effective binary diffusion coefficient is found by applying a Bruggeman correlation [12].

2.6 Cell Voltage

The cell voltage at each current density can be expressed as:

$$V_{cell} = \phi_{ca} - \phi_{an} - \Delta\phi_j + \Delta\phi_{el,Ohmic} + \Delta\phi_{io,Ohmic} \tag{23}$$

Where $\Delta\phi_{el,Ohmic}$ is the Ohmic loss across the GDL and CL due to electrical current, and $\Delta\phi_{io,Ohmic}$ is the Ohmic loss across the BPM due to ionic current.

The electrical Ohmic loss can be calculated from:

$$\Delta\phi_{el,Ohmic} = \varepsilon_{solid}^{\circ}(\rho_{el}\cdot\delta)i_{ext} \tag{24}$$

Where $\varepsilon^{\circ}_{solid}$ is the volume fraction of solid phase in the GDL or CL, ρ_{el} is the electrical resistivity of the solid phase material, and δ is the thickness of the GDL or CL.

The ionic Ohmic loss can be calculated from:

$$\Delta\phi_{io,Ohmic} = \left(\frac{1}{\sigma_{mem}} \cdot \delta_{mem}\right) i_{io} \tag{25}$$

Where σ_{mem} is the ionic conductivity of the membrane, and δ_{mem} is the thickness of the membrane.

The ionic conductivity of PEM is a function of water content and temperature [21]:

$$\sigma_{PEM} = 10^4(0.005193\lambda - 0.00326)\exp\left(1268\left(\frac{1}{303.15} - \frac{1}{T}\right)\right) \tag{26}$$

The ionic conductivity of AEM does not have a well-established correlation with water content. Therefore, data from Ref. [26] was used to establish a correlation between ionic conductivity and water activity and temperature:

$$\sigma_{AEM} = (.011a_{\mathrm{w}}^4 - 0.0064a_{\mathrm{w}}^3 + 0.022a_{\mathrm{w}}^2 + 0.00044a_{\mathrm{w}} + 8.19e^{-5}) + (.0018a_{\mathrm{w}}^4 - 0.0036a_{\mathrm{w}}^3 + 0.0025a_{\mathrm{w}}^2 - 0.00059a_{\mathrm{w}} + 3.71e^{-5})(T - 333) \tag{27}$$

2.7 Modeling Parameters

Table 1. Microstructure and Geometry Parameters

Parameter	Value	Unit
Thickness of anode GDL, $\delta_{an,GDL}$	1600	μm
Thickness of cathode GDL, $\delta_{ca,GDL}$	365	μm
Thickness of anode CL, $\delta_{an,CL}$	5	μm
Thickness of cathode CL, $\delta_{ca,CL}$	5	μm
Thickness of AEM, δ_{AEM}	25	μm
Thickness of CEM, δ_{CEM}	25	μm
Thickness of BPM junction layer, $\delta_{BPM,j}$	4	nm
Porosity of anode GDL, $\varepsilon_{an,GDL}$	0.95	-
Porosity of cathode GDL, $\varepsilon_{an,GDL}$	0.78	-
Porosity of anode CL, $\varepsilon_{an,GDL}$	0.95	-
Porosity of cathode CL, $\varepsilon_{an,GDL}$	0.5	-
Diameter of carbon particles in cathode GDL, $d_{p,GDL}$	1.466	μm
Diameter of silver particles in cathode CL, $d_{p,Ag}$	0.1	μm
Area of electrolyzer cell, A_{cell}	4	cm^2

Table 2. Electrochemical Parameters

Parameter	Value	Unit
Anode double layer capacitance, $C_{dl,an}$	100	F/m^2
Cathode double layer capacitance, $C_{dl,ca}$	100	F/m^2
Anodic exchange current density, $A_{k,an}$	1.23e-3	A/m^2
Cathodic exchange current density, $A_{k,ca}$	7.25e8	A/m^2
Anodic activation energy, $E_{A,an}$	25,000	J/mol
Cathodic activation energy, $E_{A,ca}$	100,000	J/mol
Number of electrons transferred in anodic reaction, n_{an}	2	-
Number of electrons transferred in cathodic reaction, n_{ca}	2	-

Symmetry factor of forward reaction, β_{fwd}	0.5	-
Symmetry factor of reverse reaction, β_{rev}	0.5	-

Table 3. Material Properties

Parameter	Value	Unit
Electrical conductivity of nickel, $\sigma_{el,an}$	14.3e6	S/m
Electrical conductivity of graphite, $\sigma_{el,ca}$	2e4	S/m
Ion-exchange capacity AEM, IEC_{AEM}	1.7	mol/kg
Ion-exchange capacity CEM, IEC_{CEM}	0.93	mol/kg
Dry AEM density, $\rho_{dry,AEM}$	1,200	kg/m^3
Dry CEM density, $\rho_{dry,CEM}$	1,580	kg/m^3
Concentration of AEM side chain groups, c_{AEM}	1000	mol/m^3
Concentration of CEM side chain groups, c_{CEM}	1000	mol/m^3

2.8 Boundary Conditions

At the gas channel-GDL interface a fixed species composition, temperature, and pressure are assumed. At the cathode CL-CEM interface the species flux is set to 0 except for water. In the membrane it was assumed the ionic current equals the applied current.

2.9 Numerical Method

The above equations are implemented in python and solved using Numpy's ivp solver. The relative tolerance and absolute tolerance were set to 10^{-9} and 10^{-8} respectively. The 'BDF' method was employed.

3. Results and Discussion

The water diffusion coefficient for AEM was varied between $2x10^{-9}\frac{m^2}{s}$ and $2x10^{-10}\frac{m^2}{s}$ to observe the effect on the polarization curve. The values were chosen based on the experimental measurements from Ref. [23]. The value of $n_{d,AEM}$ was fixed at 1 and the results are shown in Figure 3.

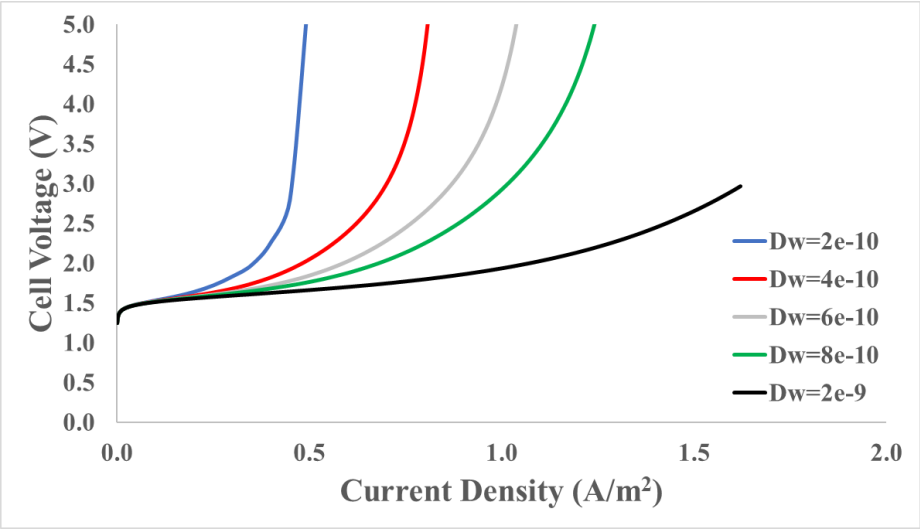

Figure 3. Polarization curves versus water diffusion coefficient in AEM.

From Figure 3, the value of the water diffusion coefficient has a drastic effect on the polarization curve. The importance of water transport to the BPM junction is also highlighted by the presence of a limiting current. At $D_{w,AEM} = 2x10^{-10}\frac{m^2}{s}$ the limiting current is $0.45\frac{A}{cm^2}$ and at $D_{w,AEM} = 2x10^{-9}\frac{m^2}{s}$ the limiting current is above $1.5\frac{A}{cm^2}$. This is due to water content in the membrane decreasing as current density increases, resulting in the ionic resistance in the membrane to increase.

The water content and the species concentration in the cathode CL layer are shown in Figures 4 and 5 respectively for $D_{w,AEM} = 6x10^{-10}\frac{m^2}{s}$ and $n_{d,AEM} = 1$.

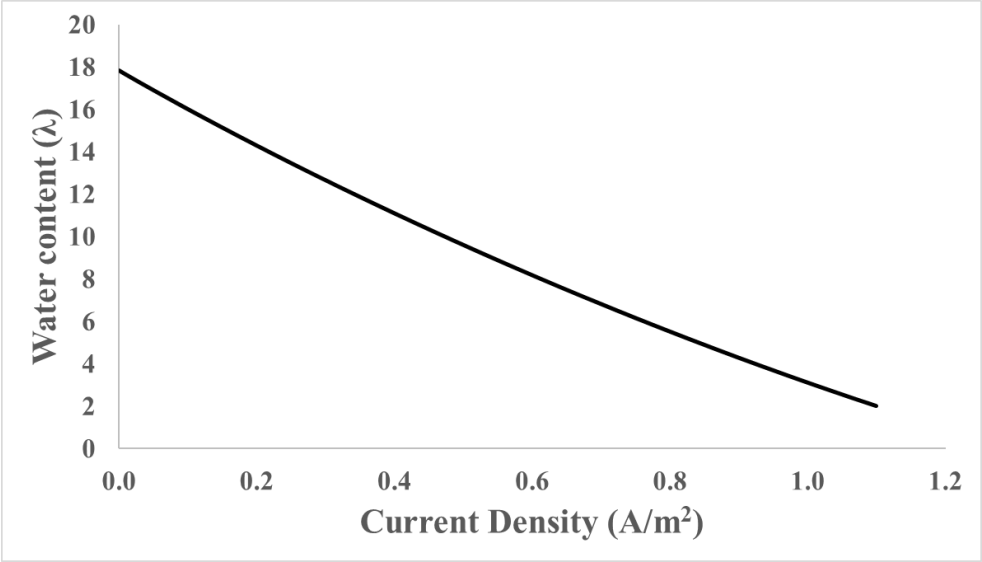

Figure 4. Water content in the BPM junction versus current density.

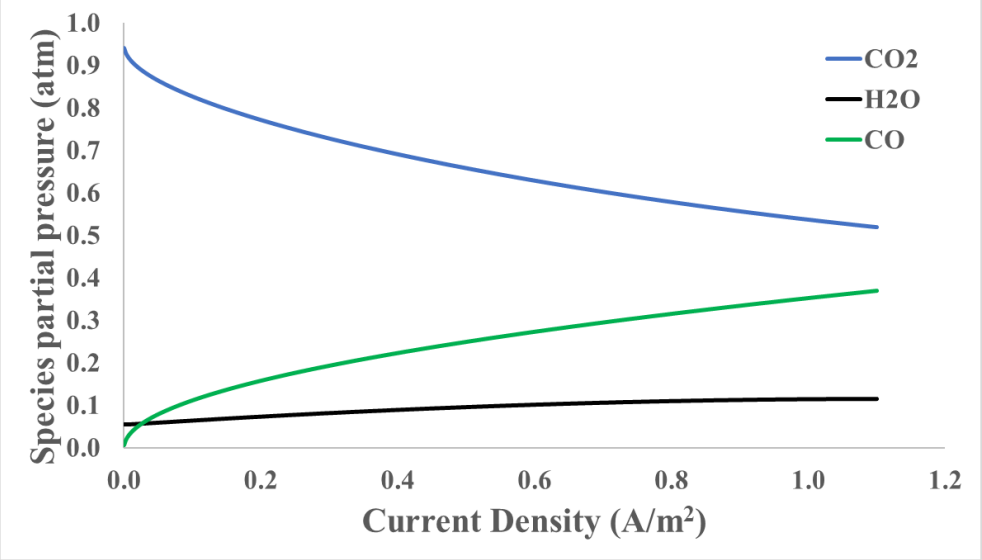

Figure 5. Species partial pressures in the cathode CL versus current density.

From Figure 6, the water content in the BPM junction significantly decreases as current density increases, thus confirming the membrane dehydration effect on the polarization curve. Furthermore, from Figure 7 the concentration of water vapor remains low despite water vapor production from the CO_2 reduction reaction. This further highlights the importance of requiring a humidified feed stream to maximize water transport to the BPM junction.

The electro-osmotic drag coefficient of the AEM was varied between 0.6 and 4 to observe the effect on the polarization curve. These values were based on the range of values reported in the literature [22,23]. The results are shown in Figure 6.

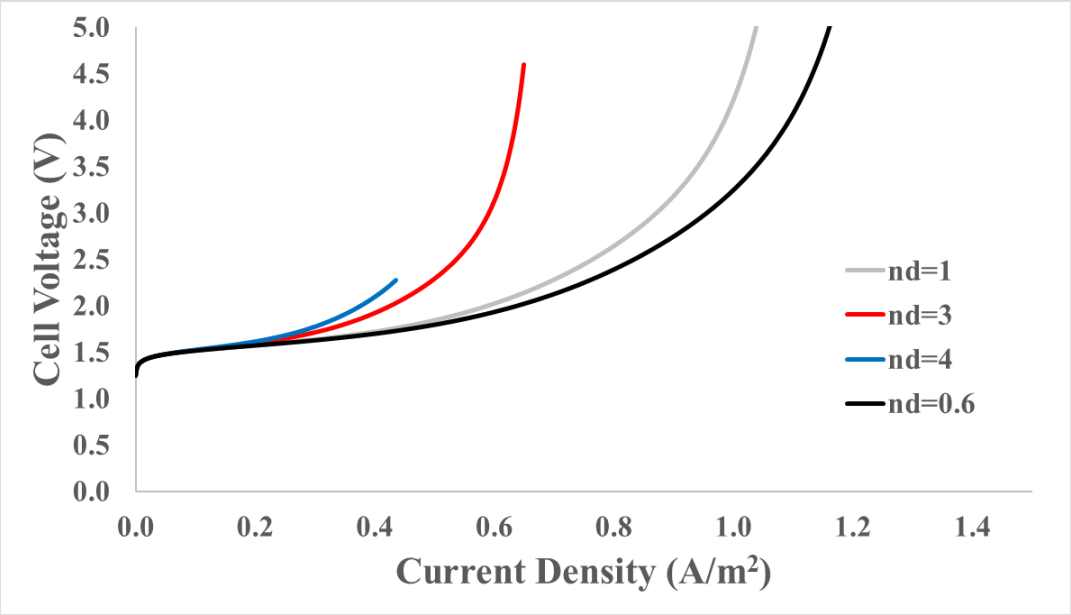

Figure 6. Polarization curves versus electro-osmotic drag coefficient in AEM.

From Figure 6, the electro-osmotic drag has a significant effect on the polarization curve. At $n_{d,AEM} = 3$ the limiting current is $0.6\frac{A}{cm^2}$ and at $n_{d,AEM} = 0.6$ the limiting current is at $1.1\frac{A}{cm^2}$. The polarization curve for $n_{d,AEM} = 4$ was truncated since the solver became unstable at high current densities.

The model includes temperature effects on the membrane properties and kinetics so the effect of temperature on the polarization curve is shown in Figure 7.

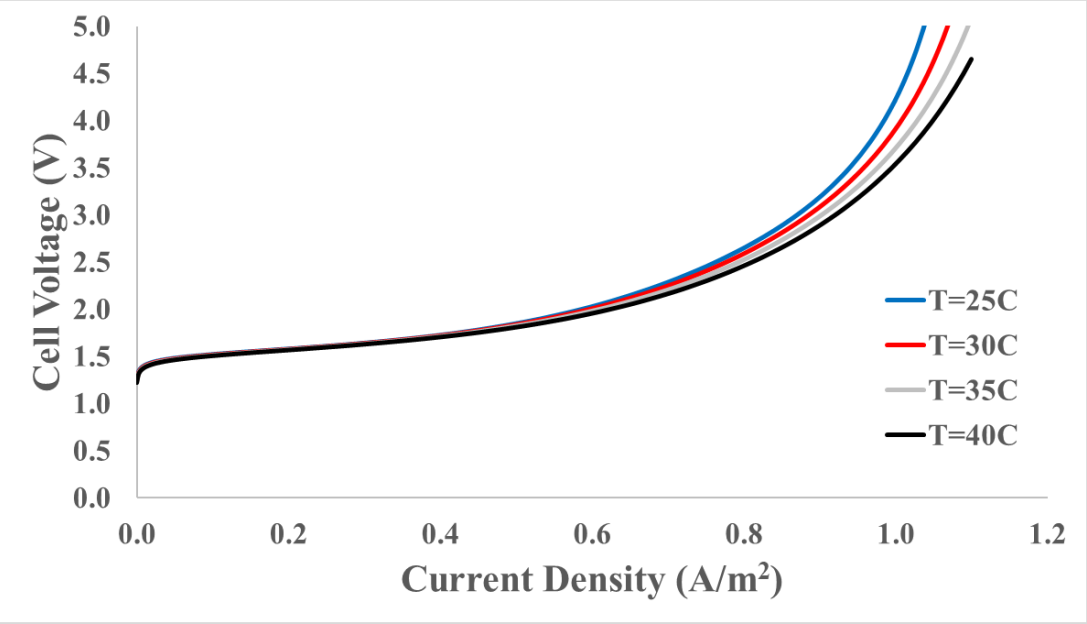

Figure 7. Polarization curves versus operating cell temperature.

From Figure 7, the increase in temperature results in higher current densities at a set cell voltage. This confirms that CO_2 electrolysis should be run at higher temperatures similar in PEM electrolyzers.

4. Conclusions

The rudimentary 1-D model was able to simulate polarization curves as a function of various membrane properties. The water diffusion coefficient and electro-osmotic drag coefficient of the AEM have significant impact on the limiting current of the electrolyzer. This was found to be due to membrane dehydration resulting in high ionic ohmic losses.

The findings highlight the need for accurate AEM property data as a function of water content when equilibrated with liquid water. The differences of values found in the literature result in limiting current differences from mA/cm^2 to A/cm^2. The model predicts that if the AEM membrane properties become favorable for water transport then industrial scale CO_2E can be achieved.

Sorry for the long report… here is a potato (and memes after references)

5. References

[1] Ritchie, H., and Roser, M., 2019, "CO2 and Other Greenhouse Gas Emissions," Our World Data.

[2] Chen, C., Khosrowabadi Kotyk, J. F., and Sheehan, S. W., 2018, "Progress toward Commercial Application of Electrochemical Carbon Dioxide Reduction," Chem, **4**(11), pp. 2571–2586.

[3] Hori, Y., 2008, "Electrochemical CO2 Reduction on Metal Electrodes," *Modern Aspects of Electrochemistry*, pp. 89–189.

[4] Calvinho, K. U. D., Laursen, A. B., Yap, K. M. K., Goetjen, T. A., Hwang, S., Murali, N., Mejia-Sosa, B., Lubarski, A., Teeluck, K. M., Hall, E. S., Garfunkel, E., Greenblatt, M., and Dismukes, G. C., 2018, "Selective CO2 Reduction to C3 and C4 Oxyhydrocarbons on Nickel Phosphides at Overpotentials as Low as 10 MV," Energy Environ. Sci., **11**(9), pp. 2550–2559.

[5] Endrődi, B., Bencsik, G., Darvas, F., Jones, R., Rajeshwar, K., and Janáky, C., 2017, "Continuous-Flow Electroreduction of Carbon Dioxide," Prog. Energy Combust. Sci., **62**, pp. 133–154.

[6] Moeller, T., Ju, W., Bagger, A., Wang, X., Luo, F., Thanh, T. N., Varela, A., Rossmeisl, J., and Strasser, P., 2019, "Efficient CO2 to CO Electrolysis on Solid Ni-N-C Catalysts at Industrial Current Densities," Energy Environ. Sci.

[7] Hoang, T. T. H., Verma, S., Ma, S., Fister, T. T., Timoshenko, J., Frenkel, A. I., Kenis, P. J. A., and Gewirth, A. A., 2018, "Nanoporous Copper-Silver Alloys by Additive-Controlled Electrodeposition for the Selective Electroreduction of CO2 to Ethylene and Ethanol," J. Am. Chem. Soc.

[8] Salvatore, D. A., Weekes, D. M., He, J., Dettelbach, K. E., Li, Y. C., Mallouk, T. E., and Berlinguette, C. P., 2018, "Electrolysis of Gaseous CO 2 to CO in a Flow Cell with a Bipolar Membrane," ACS Energy Lett., **3**(1), pp. 149–154.

[9] Verma, S., Lu, X., Ma, S., Masel, R. I., and Kenis, P. J. A., 2016, "The Effect of Electrolyte Composition on the Electroreduction of CO2 to CO on Ag Based Gas Diffusion Electrodes," Phys. Chem. Chem. Phys., **18**(10), pp. 7075–7084.

[10] Ma, S., Luo, R., Gold, J. I., Yu, A. Z., Kim, B., and Kenis, P. J. A., 2016, "Carbon Nanotube Containing Ag Catalyst Layers for Efficient and Selective Reduction of Carbon Dioxide," J. Mater. Chem. A, **4**(22), pp. 8573–8578.

[11] Li, Y. C., Zhou, D., Yan, Z., Gonçalves, R. H., Salvatore, D. A., Berlinguette, C. P., and Mallouk, T. E., 2016, "Electrolysis of CO2to Syngas in Bipolar Membrane-Based Electrochemical Cells," ACS Energy Lett., **1**(6), pp. 1149–1153.

[12] Randall, C. R., and DeCaluwe, S. C., 2020, "Physically Based Modeling of PEMFC Cathode Catalyst Layers: Effective Microstructure and Ionomer Structure–Property Relationship Impacts," J. Electrochem. Energy Convers. Storage, **17**(4), pp. 1–10.

[13] Grew, K. N., McClure, J. P., Chu, D., Kohl, P. A., and Ahlfield, J. M., 2016, "Understanding Transport at the Acid-Alkaline Interface of Bipolar Membranes," J. Electrochem. Soc., **163**(14), pp. F1572–F1587.

[14] Gupta, N., Gattrell, M., and MacDougall, B., 2006, "Calculation for the Cathode Surface Concentrations in the Electrochemical Reduction of CO2 in KHCO3 Solutions," J. Appl. Electrochem., **36**(2), pp. 161–172.

[15] Gong, J., Lu, S., Li, Q., Sui, P.-C., Xiang, Y., Djilali, N., and Li, Z., 2018, "Numerical and Experimental Investigations of Bipolar Membrane Fuel Cells: 3D Model Development and Effect of Gas Channel Width," J. Electrochem. Soc., **165**(11), pp. F994–F1001.

[16] Vermaas, D. A., Wiegman, S., Nagaki, T., and Smith, W. A., 2018, "Ion Transport Mechanisms in Bipolar Membranes for (Photo)Electrochemical Water Splitting," Sustain. Energy Fuels, **2**(9), pp. 2006–2015.

[17] Weng, L. C., Bell, A. T., and Weber, A. Z., 2019, "Towards Membrane-Electrode Assembly Systems for CO2 Reduction: A Modeling Study," Energy Environ. Sci., **12**(6), pp. 1950–1968.

[18] M. Moore et al., *J. Electrochem. Soc.*, **161**, E3125–E3137 (2014).

[19] U. Krewer, C. Weinzierl, N. Ziv, and D. R. Dekel, *Electrochim. Acta*, **263**, 433–446 (2018) [19] Vermaas, D. A., Wiegman, S., Nagaki, T., and Smith, W. A., 2018, "Ion Transport Mechanisms in Bipolar Membranes for (Photo)Electrochemical Water Splitting," Sustain. Energy Fuels, **2**(9), pp. 2006–2015.

[20] C. Weinzierl, thesis, Technical University of Braunschweig (2017).

[21] Springer, T. E., 1991, "Polymer Electrolyte Fuel Cell Model," J. Electrochem. Soc., **138**(8), p. 2334.

[22] Li, Y. S., Zhao, T. S., and Yang, W. W., 2010, "Measurements of Water Uptake and Transport Properties in Anion-Exchange Membranes," Int. J. Hydrogen Energy, **35**(11), pp. 5656–5665.

[23] Peng, J., Roy, A. L., Greenbaum, S. G., and Zawodzinski, T. A., 2018, "Effect of CO2absorption on Ion and Water Mobility in an Anion Exchange Membrane," J. Power Sources, **380**(January), pp. 64–75.

[24] Duan, Q., Ge, S., and Wang, C. Y., 2013, "Water Uptake, Ionic Conductivity and Swelling Properties of Anion-Exchange Membrane," J. Power Sources, **243**, pp. 773–778.

[25] Bird 1924- author, R. B. (Robert B., *Introductory Transport Phenomena*, Hoboken, NJ : Wiley, [2015] ©2015.

[26] Duan, Q., Ge, S., & Wang, C. Y. (2013). Water uptake, ionic conductivity and swelling properties of anion-exchange membrane. *Journal of Power Sources*, *243*, 773–778. https://doi.org/10.1016/j.jpowsour.2013.06.095

6. Memes (May-may's)


ME: IT TOOK ALL SEMESTER
BUT I THINK I UNDERSTAND SIGN
CONVENTIONS IN ELECTROCHEMISTRY.
DECALUWE: SIGNS DON'T
MATTER FAM, IT'S ALL
ARBITRARY LOL. JUST BE CONSISTENT.
imgflip.com


DeCaluwe: Never has.
Me: Wait, signs don't
matter in electrochemistry?


ELECTRICAL DOUBLE LAYER
WHEN $i_{ext} \neq i_{Far}$
imgflip.com